ISSN 0869-5911, Petrology, 2018, Vol. 26, No. 6, pp. 565–574. © Pleiades Publishing, Ltd., 2018.
Original Russian Text © Yu.V. Bataleva, Yu.N. Palyanov, Yu.M. Borzdov, I.D. Novoselov, O.A. Bayukov, N.V. Sobolev, 2018, published in Petrologiya, 2018, Vol. 26, No. 6, pp. 571–582.

Conditions of Formation of Iron–Carbon Melt Inclusions in Garnet and Orthopyroxene under *P-T* Conditions of Lithospheric Mantle

Yu. V. Bataleva[a, *], Yu. N. Palyanov[a], Yu. M. Borzdov[a], I. D. Novoselov[a, b], O. A. Bayukov[c], and N. V. Sobolev[a, b]

[a] *Sobolev Institute of Geology and Mineralogy, Siberian Branch, Russian Academy of Sciences, Novosibirsk, Russia*
[b] *Novosibirsk State University, Novosibirsk, Russia*
[c] *Kirensky Institute of Physics, Siberian Branch, Russian Academy of Sciences, Krasnoyarsk, Russia*
**E-mail: bataleva@igm.nsc.ru*

Received March 30, 2018; in final form, May 17, 2018

Abstract—Of great importance in the problem of redox evolution of mantle rocks is the reconstruction of scenarios of alteration of Fe^0- or Fe_3C-bearing rocks by oxidizing mantle metasomatic agents and the evaluation of stability of these phases under the influence of fluids and melts of different compositions. Original results of high-temperature high-pressure experiments ($P = 6.3$ GPa, $T = 1300–1500$°C) in the carbide–oxide–carbonate systems ($Fe_3C–SiO_2–(Mg,Ca)CO_3$ and $Fe_3C–SiO_2–Al_2O_3–(Mg,Ca)CO_3$) are reported. Conditions of formation of mantle silicates with metallic or metal–carbon melt inclusions are determined and their stability in the presence of CO_2-fluid representing the potential mantle oxidizing metasomatic agent are estimated. It is established that garnet or orthopyroxene and CO_2-fluid are formed in the carbide–oxide–carbonate system through decarbonation, with subsequent redox interaction between CO_2 and iron carbide. This results in the formation of assemblage of Fe-rich silicates and graphite. Garnet and orthopyroxene contain inclusions of a Fe–C melt, as well as graphite, fayalite, and ferrosilite. It is experimentally demonstrated that the presence of CO_2-fluid in interstices does not affect on the preservation of metallic inclusions, as well as graphite inclusions in silicates. Selective capture of Fe–C melt inclusions by mantle silicates is one of the potential scenarios for the conservation of metallic iron in mantle domains altered by mantle oxidizing metasomatic agents.

Keywords: high-pressure experiment, metal–carbon melt, graphite, diamond, CO_2-fluid, mantle silicates, mantle metasomatism

DOI: 10.1134/S0869591118060024

INTRODUCTION

The oxygen fugacity (fO_2) significantly affects the stability of mantle minerals, fluids and melts, thus controlling the redox state of Earth's mantle. The values of fO_2 in mantle rocks are mainly determined by speciations and concentrations of elements with variable valency, such as iron and carbon. The study of variations of oxygen fugacity in mantle rocks (Ballhaus, Frost, 1994; Frost et al., 2004; Rohrbach et al., 2007; Rohrbach, Schmidt, 2011; Shirey et al., 2013) revealed a general trend of its decrease with depth. It was experimentally demonstrated that at depths ≥250–300 km mantle is characterized by reducing environments and its fO_2 decreases to FMQ (fayalite–magnetite–quartz)–5 log. units and becomes metal-bearing. These conditions provide the stability of metallic iron, carbides, and iron–carbon alloys in mantle rocks. It is shown (Frost and McCammon, 2008; Dasgupta and Hirschmann, 2010; Marty, 2012) that the entire carbon in depleted mantle (bulk carbon contents about ~20–120 ppm) is dissolved in a metal, whereas that in undepleted mantle (300–800 ppm C) is bound in carbides (Fe_3C и Fe_7C_3). The discovery of Fe^0 and Fe_3C inclusions in diamonds serves as direct evidence for the presence of carbides and Fe^0 in lithospheric mantle (Sharp et al., 1966; Sobolev et al., 1981; Bulanova, 1995; Stachel et al., 1998; Jacob et al., 2004; Kaminsky, Wirth, 2011; Smith and Kopylova, 2014), and, in addition, indicates a possible genetic link with diamond (Rohrbach and Schmidt, 2011; Palyanov et al., 2013b; Smith et al., 2016).

In spite of the fact that fO_2 values in mantle rocks shows a general tendency to decrease with depth, the variations of oxygen fugacity in mantle are controlled by much more complex dependences (Kaminsky et al., 2015). The findings of oxidized xenoliths brought to the surface from great depths (Woodland and Koch, 2003; Creighton et al., 2009) indicate that lithospheric mantle was partially altered by mobile oxidizing metasomatic agents such as CO_2-fluid or

Table 1. Composition of systems

System	Weight, mg					Bulk composition, wt %						
	Fe_3C	SiO_2	Al_2O_3	$MgCO_3$	$CaMg(CO_3)_2$	Si	Al	Fe	Mg	Ca	C	O
Fe_3C–SiO_2–(Mg,Ca)CO_3	30.0	36.0	0.0	13.4	3.4	20.3	0.0	33.8	5.2	0.9	5.3	34.6
Fe_3C–SiO_2–Al_2O_3–(Mg,Ca)CO_3	24.6	29.5	16.8	11.0	2.8	16.3	10.5	27.1	4.1	0.7	4.2	37.1

carbonate-bearing melt. In the presence of these agents, Fe^0, carbide, and metal–carbon alloys are oxidized and involved into diamond/graphite-forming reactions (Rohrbach and Schmidt, 2011; Palyanov et al., 2013b; Ryabchikov and Kogarko, 2013). The problems of iron carbide stability under different mantle environments have been widely discussed in works dedicated to the study of the global carbon cycle and processes of diamond formation (Ryabchikov, 2009; Rybachikov and Kaminsky, 2014; Rohrbach et al., 2014; Palyanov et al., 2013b; Bataleva et al., 2017). Thus, the reconstruction of potential scenarios of the behavior of mainly metallic or carbide phases during oxidizing mantle metasomatism is of great importance for deciphering the redox evolution of mantle rocks.

Taking into account the fact that Fe^0 and Fe_3C are stable in inclusions in diamond, their preservation in other mantle minerals is also suggested. Moreover, cohenite and native iron were described as inclusions in mantle garnets from diamond-bearing rocks (Jacob et al., 2004). This work is aimed at estimating conditions of formation of metallic inclusions in mantle silicates (orthopyroxene and garnet) and assessment of their stability in the presence of CO_2-fluid as oxidizing metasomatic agent.

METHODS

Experimental determination of the conditions of formation of garnet and orthopyroxene with metallic inclusions, as well as the assessment of their stability in the presence of CO_2-fluid were carried out in the Fe_3C–SiO_2–(Mg,Ca)CO_3 and Fe_3C–SiO_2–Al_2O_3–(Mg,Ca)CO_3 systems. The experiments were performed using a multi-anvil high-pressure "split-sphere" apparatus (BARS) (Palyanov et al., 2010) at the pressure of 6.3 GPa, in the temperature range of 1300–1500°C and a run duration of 20 h. Methodical features of the assembly, design of high-pressure cell, as well as the calibration data have been published previously (Palyanov et al., 2002a; Palyanov et al., 2010; Sokol et al., 2015). As initial reagents, we used natural magnesite and dolomite (in mole proportion of 8 : 1), preliminarily synthesized iron carbide (cohenite, Fe_3C), as well as synthetic Al_2O_3 and SiO_2 (<0.01 wt % of impurities). The proportions of the staring carbonates and oxides (Table 1) were selected to form orthopyroxene + CO_2-fluid or garnet + CO_2-fluid assemblages upon reaction completion (Pal'yanov et al., 2002b). The optimal crystallization conditions of silicate phases were provided using a traditional design of the ampoule assembly, where the starting reagents were ground and homogenized. However, to simulate the interaction between carbide and silicates, some part of starting carbide was not ground, but was added into a charge as crystal fragments 300–400 μm in size, while a small excess of iron carbide with respect to oxides and carbonates was intentionally formed. Takin into account the previous experience in studying the carbides and iron-bearing oxides at mantle *P-T* conditions (Dasgupta et al., 2009; Palyanov et al., 2013b; Bataleva et al., 2015), graphite was chosen as appropriate material for ampoules.

Analytical studies were carried out at the Center for Collective Use of Multi-element and Isotopic Analysis of the Siberian Branch of the Russian Academy of Sciences (Sobolev Institute of Geology and Mineralogy, Siberian Branch, Russian Academy of Sciences, Novosibirsk). The phase and chemical compositions of run products were determined by microprobe analysis (Camebax-micro) and energy-dispersive spectroscopy (Tescan MIRA3 LMU scanning electron microscope). Silicate, oxide, metallic, and carbide phases were analyzed at an accelerating voltage of 20 kV, a beam current of 20 nA, a counting time of 10 s for each analytical line, and a beam diameter of 2–4 μm. A quenched metal–carbon melt represented by microdendritic aggregates was analyzed using increased electron beam diameter. The phase relations in samples were studied using scanning electron microscopy. The composition of iron-bearing phases, valence state of iron in them, as well as iron distribution over phases and non-equivalent sites were determined by Mossbauer spectroscopy. The measurements were carried out at room temperature on a MC-1104Ем spectrometer with a Co^{57}(Cr) source on a powdered absorber with a thickness of 1–5 mg/cm^2 (Kirensky Institute of Physics, Siberian Branch, Russian Academy of Sciences).

EXPERIMENTAL RESULTS

Experimental Results in the Fe_3C–SiO_2–(Mg,Ca)CO_3 System

Conditions and results of the experiments as well as compositions of obtained phases are shown in Tables 2–4. At the lowest temperature (1300°C), the interaction in the system leads to the formation of the orthopyrox-

Table 2. Experimental results in the carbide–oxide–carbonate systems at pressure of 6.3 GPa and run time of 20 h

Run no.	*T*, °C	Final phases
System Fe_3C–SiO_2–$(Mg,Ca)CO_3$		
970-O	1300	*Opx, Ol, Gr,* $(Fe–C)_{melt}$, $(Fe–C)_{melt}$ incl., *Ol* incl., *Gr* incl.
1029-O	1400	*Opx, Ol, Gr*, $(Fe–C)_{melt}$*, $(Fe–C)_{melt}$ incl., *Ol* incl., *Opx* incl., *Gr* incl.
936-O	1500	*Opx, Ol, Gr*, $(Fe–C)_{melt}$ incl., *Ol* incl., *Opx* incl., *Gr* incl.
System Fe_3C–SiO_2–$(Mg,Ca)CO_3$–Al_2O_3		
971-G	1300	*Grt, Opx, Gr, Mgt,* $(Fe–C)_{melt}$ incl., *Opx* incl., *Gr* incl.
1030-G	1400	*Grt, Opx, Gr*, $(Fe–C)_{melt}$ incl., *Opx* incl., *Gr* incl.
937-G	1500	*Grt, Opx, Gr*, $(Fe–C)_{melt}$ incl., *Opx* incl., *Gr* incl.

Here and in Tables 3, 4, and in Figs. 1–3: *Ol*—olivine, *Opx*—orthopyroxene, *Gr*—graphite, *Grt*—garnet, *Mgt*—magnetite, $Fe–C_{melt}$—quenched iron-carbon melt, incl.—inclusions, * single find.

Table 3. Average compositions of silicates obtained in the Fe_3C–SiO_2–$(Mg,Ca)CO_3$ system

Run no.	*T*, °C	Phase	N_A	Composition, wt %					n(O)	Formula units				
				SiO_2	FeO	MgO	CaO	total		Si	Fe	Mg	Ca	total
970-O	1300	*Opx*	12	$49.8_{(1)}$	$36.3_{(9)}$	$11.9_{(8)}$	$1.5_{(1)}$	99.6	6	$2.00_{(1)}$	$1.22_{(4)}$	$0.72_{(4)}$	$0.06_{(0)}$	4.00
		Ol	10	$32.0_{(5)}$	$56_{(1)}$	$11.0_{(5)}$	$0.07_{(1)}$	99.6	4	$1.00_{(1)}$	$1.48_{(4)}$	$0.52_{(2)}$	–	3.00
1029-O	1400	*Opx*	10	$49.6_{(9)}$	$36_{(2)}$	$12_{(2)}$	$1.5_{(10)}$	99.5	6	$1.99_{(1)}$	$1.20_{(9)}$	$0.7_{(1)}$	$0.06_{(4)}$	4.01
		Ol	8	$32.1_{(3)}$	$55.6_{(6)}$	$12.0_{(2)}$	–	99.7	4	$1.00_{(1)}$	$1.44_{(0)}$	$0.56_{(1)}$	–	3.00
936-O	1500	Opx_1	16	$48.9_{(5)}$	$38.8_{(7)}$	$10.3_{(9)}$	$1.6_{(4)}$	99.6	6	$1.99_{(1)}$	$1.32_{(4)}$	$0.63_{(5)}$	$0.07_{(2)}$	4.01
		Opx_2	6	$47.4_{(9)}$	$42.8_{(9)}$	$6.5_{(9)}$	$2.6_{(5)}$	99.4	6	$1.99_{(2)}$	$1.50_{(8)}$	$0.41_{(9)}$	$0.11_{(2)}$	4.01
		Ol	10	$32.3_{(1)}$	$55.6_{(8)}$	$11.8_{(8)}$	–	99.8	4	$1.00_{(0)}$	$1.44_{(1)}$	$0.55_{(1)}$	–	2.99

Here and in Table 4: N_A—number of analyses. Standard deviation for last digit is shown in parentheses.

ene–olivine–graphite assemblage in association with an iron–carbon melt ($Fe–C_{melt}$). The representative fragment of the sample is shown in Fig. 1a. According to the mass-balance calculations, the prevailing phase in the reaction volume (82 wt %) is orthopyroxene $Fe_{1.2}Mg_{0.7}Ca_{0.1}Si_2O_6$ (grain size of ~30–50 μm). Many orthopyroxenes contain inclusions of Fe–C melt, graphite, and Fe-rich olivine (Fig. 1b). Interstices between polycrystalline orthopyroxene aggregate are filled with Fe–C microspherules associated with graphite and olivine $Fe_{1.5}Mg_{0.5}SiO_4$ (Fig. 1a). The structure of Fe–C microspherules is represented by dendritic aggregate of Fe^0 and Fe_3C (Fig. 1c), and can be interpreted as a quenched iron–carbon melt. The quenched melt contains ~4–5 wt % carbon.

Interaction in the carbide–oxide–carbonate system at 1400°C yields orthopyroxene–olivine–graphite assemblage with diamond grown on seed crystals. The reaction volume also contains single microspherules (~10 μm) of a quenched iron–carbon melt. Obtained sample is made up of polycrystalline aggregate of orthopyroxene $Fe_{1.2}Mg_{0.7}Ca_{0.1}Si_2O_6$ (grain size of ~70–100 μm), with interstices filled with olivine ($Fe_{1.4}Mg_{0.6}SiO_4$) and graphite (Fig. 1d). Orthopyroxene contains inclusions of a quenched Fe–C melt, graphite, and olivine (Figs. 1e–1h). According to calculations, the weight proportions of obtained orthopyroxene, olivine, graphite, and Fe–C melt are 63 : 31 : 5 : 1.

The orthopyroxene–olivine–graphite assemblage was obtained at 1500°C. Orthopyroxene ($Fe_{1.3}Mg_{0.6}Ca_{0.1}Si_2O_6$) is represented by relatively large prismatic crystals 150–200 μm in size (Fig. 2a). Orthopyroxene crystals contain inclusions of a quenched Fe–C melt, graphite, as well as higher Fe orthopyroxene (Figs. 2a, 2b).

Table 4. Average compositions of silicates and oxides obtained in the Fe_3C–SiO_2–Al_2O_3–$(Mg,Ca)CO_3$ system

Run no.	T, °C	Phase	N_A	Composition, wt %						Formula units						
				SiO_2	Al_2O_3	FeO	MgO	CaO	Total	Si	Al	Fe^{2+}	Fe^{3+}	Mg	Ca	Total
971-G	1300	Grt_{rim}	12	$37.5_{(1)}$	$22.5_{(5)}$	$28.6_{(8)}$	$8.9_{(6)}$	$2.1_{(1)}$	99.5	$2.90_{(1)}$	$2.05_{(4)}$	$1.70_{(6)}$	$0.14_{(7)}$	$1.03_{(1)}$	$0.17_{(2)}$	8.00
		Grt_{core}	16	$39.0_{(5)}$	$25.8_{(4)}$	$16_{(2)}$	$14_{(1)}$	$4.2_{(7)}$	99.5	$2.86_{(2)}$	$2.23_{(5)}$	$1.0_{(1)}$	$0.03_{(2)}$	$1.58_{(5)}$	$0.33_{(1)}$	8.00
		Opx_1*	1	56.9	–	11.5	31.3	–	99.7	2.01	–	0.34	–	1.65	–	4.00
		Opx_2*	1	49.4	–	40.4	10.2	–	99.9	2.01	–	1.37	–	0.62	–	4.00
		Opx_3*	1	48.9	–	38.6	12.0	–	99.4	1.98	–	1.25	0.05	0.72	–	4.00
		Mgt	6	–	–	$90.8_{(2)}$	$7.6_{(2)}$	–	98.4	–	–	$0.56_{(1)}$	$2.00_{(0)}$	$0.43_{(1)}$	–	2.99
1030-G	1400	*Grt*	15	$38.6_{(4)}$	$21.1_{(6)}$	$28.7_{(5)}$	$9.4_{(2)}$	$1.7_{(4)}$	99.5	$2.99_{(3)}$	$1.93_{(4)}$	$1.76_{(4)}$	$0.10_{(3)}$	$1.09_{(3)}$	$0.15_{(2)}$	8.00
		Opx	7	$49.2_{(3)}$	–	$41.0_{(7)}$	$9.2_{(6)}$	–	99.5	$2.02_{(0)}$	–	$1.41_{(1)}$	–	$0.56_{(1)}$	–	4.00
937-G	1500	*Grt*	15	$39.3_{(4)}$	$21.1_{(3)}$	$28_{(1)}$	$10.0_{(6)}$	$1.7_{(4)}$	99.9	$3.02_{(1)}$	$1.91_{(2)}$	$1.74_{(9)}$	$0.05_{(2)}$	$1.14_{(3)}$	$0.14_{(1)}$	8.00
		Opx	10	$56.6_{(7)}$	–	$11_{(2)}$	$31_{(2)}$	$0.8_{(2)}$	99.5	$2.00_{(1)}$	–	$0.33_{(7)}$	–	$1.62_{(8)}$	$0.03_{(1)}$	4.00

* Non-averaged composition; Fe^{2+} and Fe^{3+} f.u., calculated by Finger method (Finger, 1972).

Experimental Results in the Fe_3C–SiO_2–Al_2O_3–$(Mg,Ca)CO_3$ System

The interaction in the carbide–oxide–carbonate system at 1300°C gives rise to garnet–orthopyroxene–graphite–magnetite assemblage (Table 2). Predominant phase in the reaction volume is garnet (grain size of ~5–40 μm) containing inclusions of a Fe–C melt, graphite, as well as Fe-rich orthopyroxene (Figs. 2c, 2d). Garnet varies in composition within $Prp_{54}Alm_{34}Ski_1Grs_{11}$–$Prp_{34}Alm_{56}Ski_5Grs_5$ (Table 3). Interstices between the polycrystalline aggregate of the garnet are filled with orthopyroxene, magnetite, and graphite. Orthopyroxene is heterogeneous in composition, with FeO content ranging from 11.5 to 40.4 wt %. Mossbauer spectroscopy established that some orthopyroxene crystals contain admixture of trivalent iron ($Fe^{3+}/\sum Fe \sim 0.04$).

At higher temperatures (1400 and 1500°C), the system generated garnet + orthopyroxene + graphite assemblage, with diamond grown on seed crystals. Garnet, the polycrystalline aggregate of which occupies most part of the ampoule, has a homogenous compositions $Prp_{35}Alm_{57}Ski_3Grs_5$ (1400°C) and $Prp_{37}Alm_{56}Ski_2Grs_5$ (1500°C) and crystal size ~30–70 μm. The garnet contains inclusions of a quenched Fe–C melt, graphite, as well as Fe-rich orthopyroxene. Fine-grained orthopyroxene + graphite aggregate fills interstices in the garnet matrix. Orthopyroxenes obtained at 1400°C and 1500°C, in composition correspond to $Fe_{1.41}Mg_{0.56}Si_{2.02}O_6$ and $Fe_{0.33}Mg_{1.62}Ca_{0.03}Si_2O_6$.

INCLUSIONS IN SILICATES

Inclusions in the orthopyroxene and garnet were established within the entire temperature range and consist of a quenched Fe–C melt, graphite, as well as Fe-rich olivine and orthopyroxene (Figs. 1b, 1e–1h, 3). In addition to monophase inclusions of a quenched melt, graphite, and olivine, many orthopyroxene crystals contain polyphase inclusions of $Fe–C_{melt}$ + graphite, $Fe–C_{melt}$ + graphite + olivine, olivine + graphite, $Fe–C_{melt}$ + graphite + Fe-orthopyroxene, and $Fe–C_{melt}$ + graphite + olivine + Fe-orthopyroxene (Figs. 1e–1h).

Inclusions of an Iron–Carbon Melt in Orthopyroxene

Inclusions of a quenched Fe–C melt obtained at 1300 and 1400°C are mainly microspherules (Figs. 1b, 1e–1h, 3a). They contain 4–6 wt % C, which in general corresponds to melt forming in the system. It is established that the largest single inclusions (10–17 μm) are restricted to the central parts of host crystals, while periphery of the crystal is saturated in the finest (3–5 μm) numerous inclusions. The structure of the widest spread polyphase inclusions containing a Fe–C melt is shown in Figs. 1e, 1f. Inclusions consisting of microspherules of a quenched melt ± graphite were

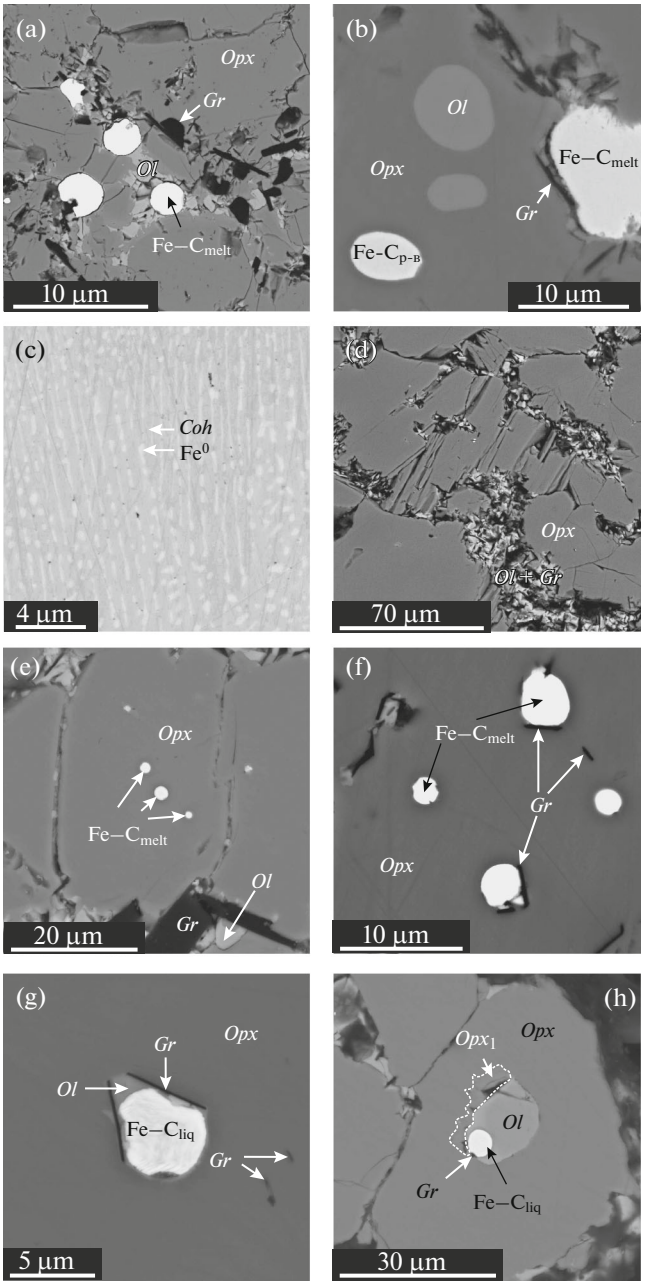

Fig. 1. SEM-microimage (BSE) of polished fragments of obtained samples (Fe_3C–SiO_2–$(Mg,Ca)CO_3$ system, P = 6.3 GPa, 20 h). (a) Polycrystalline orthopyroxene aggregate with interstitial Fe-rich olivine, graphite, and microspherules of a quenched Fe-C melt (1300°C); (b) inclusions of $Fe–C_{melt}$, Fe-rich olivine, and graphite in orthopyroxene (1300°C); (c) structure of $Fe–C_{melt}$ (1300°C); (d) polycrystalline aggregate of orthopyroxene with interstitial Fe-rich olivine and graphite (1400°C); (e) $Fe–C_{melt}$ microspherules in orthopyroxene (1400°C); (f) inclusions of $Fe–C_{melt}$ and graphite in orthopyroxene (1400°C); (g) inclusions of $Fe–C_{melt}$, Fe-rich olivine, and graphite in orthopyroxene (1400°C); (h) polyphase inclusion consisting of $Fe–C_{melt}$, Fe-rich olivine and graphite surrounded by a rim of Fe-rich olivine.

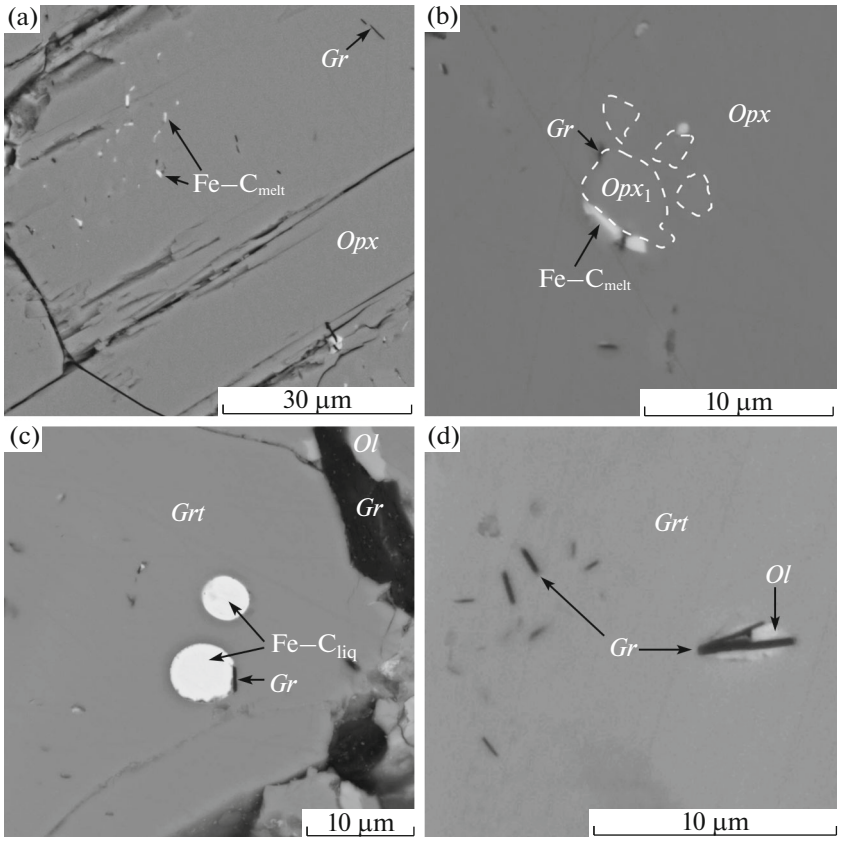

Fig. 2. SEM microimages (BSE) of polished fragments of obtained samples. (a, b) $Fe_3C–SiO_2–(Mg,Ca)CO_3$ system, T = 1500°C, (c, d) $Fe_3C–SiO_2–(Mg,Ca)CO_3–Al_2O_3$ system, T = 1300°C: (a, b) orthopyroxene crystal with lens-like inclusions of quenched iron–carbon melt (Fe–C$_{melt}$); (c) inclusions of Fe–C$_{melt}$ in garnet; (d) graphite and olivine inclusions in garnet (1300°C).

found in more than 80% orthopyroxene crystals and are the widest spread. The representative microimage of the second in abundance inclusion type is shown in Fig. 1g. These inclusions consist of microspherules of a quenched Fe–C melt, which is partially or completely rimmed by Fe-rich olivine, as well as by lamellar graphite. In some cases, these inclusions also contain Fe-rich orthopyroxene (Fig. 1h). The Fe–C inclusions obtained at 1500°C are only partially represented by microspherules, most of which have the lens-like shape (Figs. 2a, 2b). These lens-like inclusions associate with inclusions of Fe-rich orthopyroxene and graphite (Figs. 2a, 2b).

Inclusions of Graphite and Fe-Rich Silicates in Orthopyroxene

Graphite inclusions are represented by lamellae 3–5 μm in size. They are present in orthopyroxene as monophase inclusions (Fig. 3d) and occur also in the polyphase inclusions, in association with a quenched Fe–C melt and/or with olivine (Figs. 1b, 1f–1h, 3c, 3d). Inclusions of Fe-rich olivine were established in orthopyroxenes only in experiments conducted at 1300 and 1400°C. They are the largest in size, reaching 10 μm, sometimes 20 μm (Figs. 1b, 3c). The characteristic feature of these inclusions is their rounded morphology (Fig. 1b). Their compositions correspond to $Fe_{1.5}Mg_{0.5}SiO_4$ (1300°C) and $Fe_{1.4}Mg_{0.6}SiO_4$ (1400°C). The Fe-rich orthopyroxene at 1400°C was found only as single polyphase inclusions (Fig. 1h), and is one of the most abundant inclusions in orthopyroxene at 1500°C (Fig. 2b). The composition of these inclusions corresponds to $Fe_{1.5}Mg_{0.3}Ca_{0.2}Si_2O_6$, while their size on average is 10 μm.

Inclusions in Garnet

Inclusions in garnet were found within a temperature range from 1300 to 1500°C and consist of a quenched Fe–C melt, graphite, as well as Fe-rich orthopyroxene (Figs. 2c, 2d). All above mentioned phases occur both in monophase and polyphase inclusions: Fe–C$_{melt}$ + graphite, graphite + Fe-orthopyroxene, Fe–C$_{melt}$ + graphite + Fe-orthopyroxene (Figs. 2c, 2d). Unlike similar inclusions in orthopy-

roxene obtained in the $Fe_3C–SiO_2–(Mg,Ca)CO_3$ system, the characteristic features of inclusions in garnet are temperature-independent. It is established that the inclusions of a quenched Fe–C melt (C ~ 4–5 wt %) are present in garnet crystals as microspherules 2–3 μm in size. Graphite in the inclusions is represented by lamellae up to 7 μm in size. The Fe-rich orthopyroxene ($Fe_{1.22}Mg_{0.34}Ca_{0.33}Si_2O_6$) forms equant inclusions up to 10 μm in size.

DISCUSSION

Formation of Silicates, Graphite (± Diamond) and Iron–Carbon Melt

Results of performed experiments indicate that at 1300–1500°C the system experience a complete decarbonation, with formation of orthopyroxene or garnet and release of CO_2-fluid (1)–(2), which in turn is involved in the redox interaction with iron carbide (3):

$$2(Mg,Ca)CO_3 + 2SiO_2 \rightarrow (Mg,Ca)_2Si_2O_6 + 2CO_2, \quad (1)$$

$$3(Mg,Ca)CO_3 + Al_2O_3 + 3SiO_2 \rightarrow (Mg,Ca)_3Al_2Si_3O_{12} + 3CO_2, \quad (2)$$

$$3Fe_3C + 3CO_2 \rightarrow 6FeO_{\text{in silicates}} + 3Fe\text{-}C_{melt} + 5C^0. \quad (3)$$

The redox interaction (3) results in the formation of elementary carbon (graphite), Fe–C melt, as well as FeO, which does not form own phase but is incorporated into silicates: orthopyroxene, garnet, and olivine. New portions of CO_2-fluid forming at the next stages of experiments interact with a Fe–C melt to produce carbon:

$$3Fe–C_{melt} + 3CO_2 \rightarrow 6FeO_{\text{in silicates}} + 4C^0. \quad (4)$$

Crystallization of metastable graphite in the diamond stability field in the given case could be also caused by inhibiting influence of impurities, for instance, oxygen and nitrogen, which were absorbed on the initial reagents. Study of diamond crystallization in the metal–carbon systems in the presence of impurities (Palyanov et al., 2010, 2013b) showed that ~0.48 wt % H_2O or ~0.1 wt % nitrogen in a Fe–Ni–C melt are sufficient to form the metastable graphite in the diamond stability field. The crystallization of the metastable graphite instead of diamond was also established in other model systems, for instance, in the carbonate–silicate (Palyanov et al., 2001) and fluid (Palyanov et al., 2000) systems usually at relatively low temperatures.

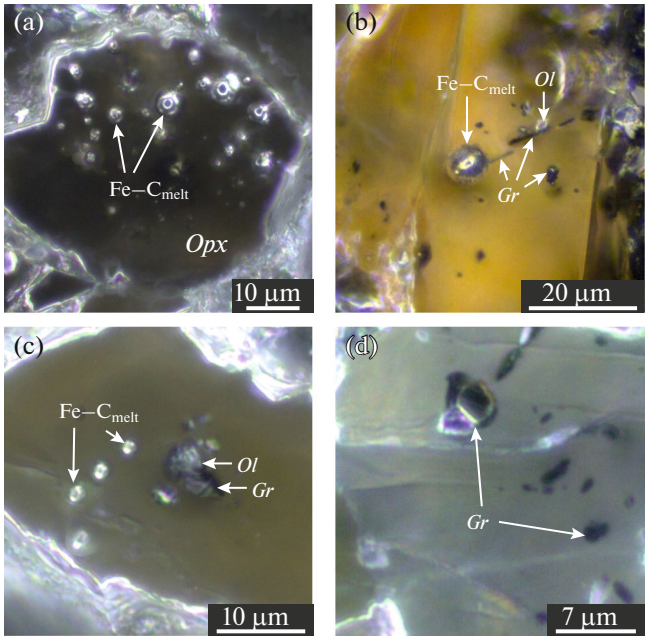

Fig. 3. Optical microimages (reflected light, dark field regime) of inclusions in orthopyroxene (T = 1400°C). (a) microspherules of a quenched Fe–C melt; (b) microspherules of Fe–C, lamellar graphite and Fe-rich olivine; (c) microspherules of quenched Fe–C melt and Fe-rich olivine; (d) graphite inclusions of diverse morphology.

Formation of Inclusions in Orthopyroxene and Garnet

The discovery of inclusions in both central and marginal zones of garnet and orthopyroxene indicates that they were entrapped at all stages of decarbonation. At the same time, the confinement of the largest Fe–C melt inclusions to the central parts of the silicate crystals, and the smallest ones, to the periphery, reflects a change in the degree of decarbonation and reaction (4) depth at different stages of the experiment. According to the redox reaction (4), the formation of the first portions of CO_2 fluid at the initial stage of experiments was accompanied by the oxidation of much lower amount of Fe–C melt than during complete decarbonation of the system at the final stages, which directly affected the size of entrapped microspherules.

The bulk composition of the inclusions shows that > 80% of them are represented by only Fe–C melt or Fe–C melt + graphite. At the same time, it was established that the predominant component in the crystallization environment was CO_2-fluid, whose inclusions were found neither in garnet nor in orthopyroxene. For instance, Figure 3a shows that one orthopyroxene crystal (about 60 μm in size) can entrap over 45 inclusions 1–8 μm in size, which contain only a Fe–C melt. Obtained data point to a selective capture of mainly metallic melt by silicates during their crystallization according to decarbonation reactions.

The detailed study of the composition and structure of polyphase inclusions showed that some of them changed their phase composition after entrapment. The entrapment of several drops of a Fe–C melt together with small amount of CO_2-fluid into orthopyroxene or garnet during crystallization led to the interaction between these fO_2-contrasting phases, Fe–C melt and fluid, and formation of a peculiar type of inclusions (Fig. 1h). Interaction between a Fe–C melt and CO_2-fluid in the inclusion results in the graphite crystallization and formation of FeO, which interacts with host orthopyroxene to produce two new silicate phases: Fe-rich orthopyroxene and Fe-rich olivine. It is most probable that the entrapment of a Fe–C melt and CO_2 inclusions is accompanied by the formation of thin FeO film around melt, thus retarding the redox reaction between the melt and fluid. In addition to phase composition, these inclusions are also characterized by an important feature: rounded morphology of newly formed olivine (Figs. 1b, 1h), which presumably inherits the shape of initial drop of Fe–C melt. This type of inclusions is also peculiar in the formation of Fe-rich orthopyroxene at the host crystal/inclusion contact. Numerous inclusions obtained during experiment at 1500°C and consisting of lenses of Fe–C melt, graphite, and Fe-rich orthopyroxene were presumably formed by the same manner. The rapid growth of orthopyroxene crystals could result in the entrapment of inclusions where CO_2-fluid predominates over Fe–C melt. The redox interactions in such inclusions could produce polyphase inclusions consisting of Fe–C lenses, and graphite lamellae and Fe-rich orthopyroxene. It should be noted that in spite of the evidence for the redox reactions within individual inclusions, the majority of inclusions show no signs of influence of CO_2-fluid. Thus, it was experimentally proved that garnet and orthopyroxene could serve as reliable "screen" between metallic or carbide phases and fugacity-contrasting mantle metasomatic agents.

Conditions of Formation of Silicates with Inclusions of an Iron–Carbon Melt and Graphite under Natural Lithospheric Mantle Setting

According to the modern concept, reduced metal-bearing mantle contains about 1400 ppm Fe^0 (Rohrbach et al., 2007), which depending on carbon content and *P-T* conditions, occurs as metal, Fe–C melt, or carbide (Frost and McCammon, 2008; Dasgupta and Hirschmann, 2010; Marty, 2012). It is suggested that subduction of crustal material results in the interaction of metallic or carbide phases with oxidized slab, which is a source of carbonates and CO_2-fluid (Dobretsov, 2010; Kogarko and Ryabchikov, 2013; Perchuk et al., 2013). One of the most abundant types of subduction-related reactions is decrabonation during interaction of carbonate material with mantle oxides or silicates. However, subducted Mg–Ca carbonates could be stable up to the lower mantle depths (Brenker et al., 2007; Boulard et al., 2011; Merlini et al., 2012; Oganov et al., 2013). As shown in (Berman, 1991; Palyanov et al., 2007; Martin and Hammouda, 2011; Bataleva et al., 2016), the presence of iron could initiate decarbonation at much lower temperatures and serve as peculiar "trigger" for the generation of Fe-rich silicates in association with CO_2-fluid. It is established that experimentally simulated decarbonation with a participation of metallic iron or carbide could locally occur under natural conditions of subduction of oxidized material into reduced mantle.

CONCLUSIONS

Thus, experimental modeling of the interaction in the carbide–oxide–carbonate system made it possible to determine the conditions of formation of Fe–C melt and graphite inclusions in mantle silicates and to estimate their stability in the presence of CO_2-fluid, the potential oxidizing mantle metasomatic agent, under lithospheric mantle conditions. It is established that the rapid crystallization of orthopyroxene and garnet under mantle pressures and temperatures could provide a selective capture of inclusions of a metal–carbon melt and graphite. The presence of interstitial CO_2-fluid does not provide the conservation of metallic inclusions, as well as graphite inclusions in silicates. It is experimentally proved that the selective capture of inclusions of metallic melt and graphite by silicates that are stable in the presence of CO_2-fluid could be favorable for the conservation of metallic phase and C^0 in mantle domains altered by oxidizing metasomatic agents.

ACKNOWLEDGMENTS

This work was supported by the Russian Foundation for Basic Research (project no. 16-35-60024) and a State Assignment (project no. 0330-2016-0007).

REFERENCES

Ballhaus, C. and Frost, B.R., The generation of oxidized CO_2-bearing basaltic melts from reduced CH_4-bearing upper mantle sources, *Geochim. Cosmochim. Acta,* 1994, vol. 58, pp. 4931–4940.

Bataleva, Yu.V., Palyanov, Yu.N., Sokol, A.G., et al., The role of rocks saturated with metallic iron in the formation of ferric carbonate–silicate melts: experimental modeling under lithospheric mantle *P-T*-conditions, *Russ. Geol. Geophys.,* 2015, vol. 56, nos. 1–2, pp. 143–154.

Bataleva, Y.V., Palyanov, Y.N., Sokol, A.G., et al., Wustite stability in the presence of a CO_2-fluid and a carbonate–silicate melt: implications for the graphite/diamond formation and generation of Fe-rich mantle metasomatic agents, *Lithos,* 2016, vol. 244, pp. 20–29.

Bataleva, Y.V., Palyanov, Y.N., Borzdov, Y.M., et al., Iron carbide as a source of carbon for graphite and diamond formation under lithospheric mantle *P-T* parameters, *Lithos,* 2017, vol. 286-287, pp. 151–161.

Berman, R.G., Thermobarometry using multiequilibrium calculations: a new technique with petrologic applications, *Can. Mineral.,* 1991, vol. 29, pp. 833–855.

Boulard, E., Gloter, A., Corgne, A., et al., New host for carbon in the deep Earth, *Proceed. Natl. Acad. Sci. USA,* 2011, vol. 108, no. 13, pp. 5184–5187.

Brenker, F.E., Vollmer, C., Vincze, L., et al., Carbonates from the lower part of transition zone or even the lower mantle, *Earth Planet. Sci. Lett.,* 2007, vol. 260, pp. 1–9.

Bulanova, G.P., The formation of diamond, *J. Geochem. Explor.,* 1995, vol. 53, pp. 2–23.

Creighton, S., Stachel, T., Matveev, S., et al., Oxidation of the Kaapvaal lithospheric mantle driven by metasomatism, *Contrib. Mineral. Petrol.,* 2009, vol. 157, pp. 491–504.

Dasgupta, R., Buono, A., Whelan, G., and Walker, D., High-pressure melting relations in Fe–C–S systems: implications for formation, evolution, and structure of metallic cores in planetary bodies, *Geochim. Cosmochim. Acta,* 2009, vol. 73, pp. 6678–6691.

Dasgupta, R. and Hirschmann, M.M., The deep carbon cycle and melting in Earth's interior, *Earth Planet. Sci. Lett.,* 2010, vol. 298, pp. 1–13.

Dobretsov, N.L., Distinctive petrological, geochemical, and geodynamic features of subduction-related magmatism, *Petrology,* 2010, vol. 18, no. 1, pp. 84–105.

Frost, D.J., Liebske, C., Langenhorst, F., and McCammon, C.A., Experimental evidence for the existence of iron-rich metal in the Earth's lower mantle, *Nature,* 2004, vol. 428, pp. 409–412.

Frost, D.J. and McCammon, C.A., The redox state of Earth's mantle, *Annu. Rev. Earth Planet. Sci.,* 2008, vol. 36, pp. 389–420.

Jacob, D.E., Kronz, A., and Viljoen, K.S., Cohenite, native iron and troilite inclusions in garnets from polycrystalline diamond aggregates, *Contrib. Mineral. Petrol.,* 2004, vol. 146, issue 5, pp. 566–576.

Kaminsky, F.V. and Wirth, R., Iron carbide inclusions in lower-mantle diamond from Juina, Brazil, *Can. Mineral.,* 2011, vol. 49, pp. 555–572.

Kaminsky, F.V., Ryabchikov, I.D., McCammon, C.A., et al., Oxidation potential in the Earth's lower mantle as recorded by ferropericlase inclusions in diamond, *Earth Planet. Sci. Lett.,* 2015, vol. 417, pp. 49–56.

Kogarko, L.N. and Ryabchikov, I.D., Diamond potential versus oxygen regime of carbonatites, *Petrology,* 2013, vol. 21, no. 4, pp. 316–335.

Martin, A.M. and Hammouda, T., Role of iron and reducing conditions on the stability of dolomite + coesite between 4.25 and 6 GPa—a potential mechanism for diamond formation during subduction, *Eur. J. Mineral,* 2011, vol. 23, pp. 5–16.

Marty, B., The origins and concentrations of water, carbon, nitrogen and noble gases on Earth, *Earth Planet. Sci. Lett.,* 2012, vol. 313–314, pp. 56–66.

Merlini, M., Crichton, W.A., Hanfland, M., et al., Structures of dolomite at ultrahigh pressure and their influence on the deep carbon cycle, *Proceed. Natl. Acad. Sci. USA,* 2012, vol. 109, no. 34, pp. 13509–13514.

Oganov, A.R., Hemley, R.J., Hazen, R.M., and Jones, A.P., Structure, bonding and mineralogy of carbon at extreme conditions, *Rev. Mineral. Geochem.,* 2013, vol. 75, no. 1, pp. 47–77.

Palyanov, Yu.N., Shatskii, V.S., Sokol, A.G., et al., Crystallization of metamorphic diamond: an experimental modeling, *Dokl. Earth Sci.,* 2001, vol. 380, pp. 935–938.

Pal'yanov, Yu.N., Sokol, A.G., Khokhryakov, A.F., et al., Diamond and graphite crystallization in COH fluid at *P-T* parameters of the natural diamond formation, *Dokl. Earth Sci.,* 2000, vol. 375A, no. 9, pp. 1395–1398.

Pal'yanov, Y.N., Sokol, A.G., Borzdov, Y.M., and Khokhryakov, A.F., Fluid-bearing alkaline carbonate melts as the medium for the formation of diamonds in the earth's mantle: an experimental study, *Lithos,* 2002a, vol. 60, nos. 3–4, pp. 145–159.

Palyanov, Y.N., Sokol, A.G., Borzdov, Yu.M., et al., Diamond formation through carbonate-silicate interaction, *Am. Mineral.,* 2002b, vol. 87, pp. 1009–1013.

Palyanov, Y.N., Borzdov, Y.M., Bataleva, Y.V., et al., Reducing role of sulfides and diamond formation in the earth's mantle, *Earth Planet. Sci. Lett.,* 2007, vol. 260, pp. 242–256.

Palyanov, Y.N., Borzdov, Y.M., Khokhryakov, A.F., et al., Effect of nitrogen impurity on diamond crystal growth processes, *Cryst. Growth Design,* 2010, vol. 10, no. 7, pp. 3169–3175.

Palyanov, Y.N., Khokhryakov, A.F., Borzdov, Y.M., and Kupriyanov, I.N., Diamond growth and morphology under the influence of impurity adsorption, *Cryst. Growth Des.,* 2013a, vol. 13, no. 12, pp. 5411–5419.

Palyanov, Y.N., Bataleva, Y.V., Sokol, A.G., et al., Mantle-slab interaction and redox mechanism of diamond formation, *Proceed. Natl. Acad. Sci. USA,* 2013b, vol. 110, no. 51, pp. 20408–20413.

Perchuk, A.L., Shur, M.Yu., Yapaskurt, V.O., and Podgornova, S.T., Experimental modeling of mantle metasomatism coupled with eclogitization of crustal material in a subduction zone, *Petrology,* 2013, vol. 21, no. 6, pp. 579–598.

Rohrbach, A., Ballhaus, C., Golla-Schindler, U., et al., Metal saturation in the upper mantle, *Nature,* 2007, vol. 449, pp. 456–458.

Rohrbach, A. and Schmidt, M.W., Redox freezing and melting in the earth's deep mantle resulting from carbon–iron redox coupling, *Nature,* 2011, vol. 472, pp. 209–212.

Rohrbach, A., Ghosh, S., Schmidt, M.W., et al., The stability of Fe–Ni carbides in the Earth's mantle: evidence for a low Fe–Ni–C melt fraction in the deep mantle, *Earth Planet. Sci. Lett.,* 2014, vol. 388, pp. 211–221.

Ryabchikov, I.D., Mechanisms of diamond formation: reduction of carbonates or partial oxidation of hydrocarbons, *Dokl. Earth Sci.,* 2009, vol. 429, pp. 1346–1349.

Ryabchikov, I.D. and Kaminsky, F.V., Physicochemical parameters of the material of mantle plumes: evidence from the thermodynamic analysis of mineral inclusions in sub-

lithospheric diamond, *Geochem. Int.,* 2014, vol. 52, no. 11, pp. 903–911.

Ryabchikov, I.D. and Kogarko, L.N., Physicochemical parameters of deep-seated mantle plumes, *Russ. Geol. Geophys.,* 2016, vol. 57, no. 5, pp. 687–697.

Sharp, W.E., Pyrrhotite, a common inclusion in south African diamonds, *Nature,* 1966, vol. 21, no. 1, pp. 402–403.

Shirey, S.B., Cartigny, P., Frost, D.G., et al., Diamonds and the geology of mantle carbon, *Rev. Mineral. Geochem.,* 2013, vol. 75, pp. 355–421.

Smith, E.M. and Kopylova, M.G., Implications of metallic iron for diamonds and nitrogen in the sublithospheric mantle, *Can. J. Earth Sci.,* 2014, vol. 51, no. 5, pp. 510–516.

Smith, E.M., Shirey, S.B., Nestola, F., et al., Large gem diamonds from metallic liquid in Earth's deep mantle, *Science,* 2016, vol. 354, no. 6318, pp. 1403–1405.

Sobolev, N.V., Efimova, E.S., and Pospelova, L.H., Native iron in diamonds of Yakutia and its paragenesis, *Geol. Geofiz.,* 1981, no. 12, pp. 25–28.

Sokol, A.G., Borzdov, Y.M., Palyanov, Y.N., and Khokhryakov, A.F., High-temperature calibration of a multi-anvil high pressure apparatus, *High Pres. Res.,* 2015, vol. 35, no. 2, pp. 139–147.

Stachel, T., Harris, J.W., and Brey, G.P., Rare and unusual mineral inclusions in diamonds from Mwadui, Tanzania, *Contrib. Mineral. Petrol.,* 1998, vol. 132, no. 1, pp. 34–47.

Woodland, A.B. and Koch, M., Variation in oxygen fugacity with depth in the upper mantle beneath the Kaapvaal Craton, Southern Africa, *Earth Planet. Sci. Lett.,* 2003, vol. 214, pp. 295–310.

Translated by M. Bogina